JOURNAL OF PROPULSION AND POWER
Vol. 15, No. 3, May–June 1999

Liquid Jet Atomization in a Compressible Gas Stream

Tingbao Chen* and Xianguo Li†
University of Waterloo, Waterloo, Ontario N2L 3G1, Canada

A linear stability analysis has been carried out for a viscous liquid jet issued into an inviscid moving compressible gas medium with three-dimensional disturbances. The disturbances are allowed to grow both temporally and spatially. It is found that gas compressibility has a profound and significant influence on the stability of the liquid jet, especially at high Mach numbers. It is also shown that three-dimensional disturbances play an important role in the atomization process, in particular, for flows at high Weber numbers. Under certain conditions, three-dimensional sinuous disturbances even become more unstable than the corresponding two-dimensional axisymmetrical (varicose) disturbances because of the effects of liquid viscosity. Effects of other parameters such as gas-to-liquid density ratio and gas velocity are also investigated.

Nomenclature

a = unperturbed liquid jet radius
c = speed of sound for the gas phase
I_n = modified Bessel function of the first kind with order n
i = $\sqrt{-1}$
K_n = modified Bessel function of the second kind with order n
k = axial wave number
M_a = U_l/c, the Mach number of the ambient gas with respect to a frame of reference
m = ka
n = azimuthal wave number
$\boldsymbol{n}$ = unit vector normal to the liquid–gas interface, pointing into the gas phase
P = pressure
p = pressure perturbation
q_a = $\sqrt{\{m^2 + [\Omega/\sqrt{(We)} + imU]^2 M_a^2\}}$
q^2 = $k^2 + (\omega + ikU_g)^2/c^2$
r = radial coordinate
s_a = $\sqrt{(m^2 + \Omega_1/Z)}$
s^2 = $k^2 + (\omega + ikU_l)/\nu_l$
t = time
U = velocity or U_g/U_l, the velocity ratio of gas to liquid
$\boldsymbol{U}$ = velocity vector
$\boldsymbol{u}$ = velocity perturbation
We = $\rho_l U_l^2 a/\sigma$, the liquid Weber number
Z = $\mu_l/(\rho_l a\sigma)^{1/2}$, the Ohnesorge number
z = axial coordinate
Δ, Δ_1 = defined in Eqs. (24) and (25)
η = surface displacement from the equilibrium position $r = a$
η_0 = initial disturbance amplitude
θ = azimuthal coordinate
μ = dynamic viscosity
ν = kinematic viscosity
ξ = radial position of the gas–liquid interface
ρ = density or $\bar{\rho}_g/\bar{\rho}_l$, the density ratio of gas-to-liquid
ρ' = density perturbation
σ = surface tension
υ = stress tensor
Ω = $\omega(\rho_l a^3/\sigma)^{1/2}$
Ω_1 = $\Omega + im\sqrt{(We)}$
Ω_2 = $\Omega + imU\sqrt{(We)}$
ω = eigenfrequency

Subscripts

g = gas-phase property
j = g or l
l = liquid-phase property
r = radial direction
z = axial direction
θ = azimuthal direction

Superscripts

$\bar{}$ = base flowfield
$\tilde{}$ = pre-exponential function, defined in Eq. (21)

Introduction

ATOMIZATION of a circular liquid jet in a gas medium is a process of instability development and subsequent disintegration of the liquid jet into droplets of diameters much smaller than that of the jet. This process is widely used in practical applications such as fuel injection in diesel engines and scramjet combustors. A good understanding of the fundamental mechanism of atomization is essential to the performance improvement of various industrial processes in which liquid atomization is employed. Extensive studies on the mechanism of atomization have been conducted over the past century, and an extensive review of the subject has been given by Lefebvre.[1] The liquid-jet atomization process has been investigated theoretically as a direct result of aerodynamic instability resulting from either temporally or spatially growing disturbances. In most of these studies, both liquid and ambient gas phases have been assumed incompressible.

Recently, high-pressure fuel injection in diesel engines has been attempted in the effort to reduce pollutant emission and to enhance fuel efficiency. In scramjet combustors, liquid fuel is injected into a supersonic gas stream. Experimental evidences indicate that the compressibility effect of the ambient gas phase may become significant.[2] As a result, Zhou and Lin[3,4] studied the effect of compressibility on the absolute and convective instability of an inviscid liquid jet in an inviscid gas medium. Their results reveal that the gas-phase compressibility may have considerable influence on the characteristics and growth of instability, whereas the effect of liquid-phase compressibility is very minimal, if it is noticeable at all. Similarly, Li and Kelly[5] analyzed the temporal and spatial instability of an inviscid incompressible liquid jet in an inviscid compressible gas medium. Lian and Reitz[6] also investigated the effect of compressibility and vaporization on the liquid-jet atomization process.

Received Sept. 22, 1997; revision received July 10, 1998; accepted for publication Sept. 11, 1998.

*Research Assistant, Department of Mechanical Engineering; currently Senior Engineer at Electrohome Limited, Projection Systems, 809 Wellington Street North, Kitchener, Ontario N2G 4J6, Canada.

†Associate Professor, Department of Mechanical Engineering. Member AIAA.

However, most of the previous theoretical studies just discussed have neglected viscous effects and considered the atomization process a result of the growth of two-dimensional axisymmetrical (varicose) disturbances. Experimental observations[1] have long since indicated the importance of three-dimensional disturbance growth on the jet disintegration process. Li[7] was the first to consider the full effect of three-dimensional disturbances in his studies on viscous incompressible liquid jets in an inviscid incompressible gas medium. It was shown that three-dimensional disturbances are relatively unimportant at low Weber numbers, but their growth rate becomes almost identical to that of varicose disturbances at large Weber numbers. At high Weber numbers and large Ohnesorge numbers, three-dimensional sinuous disturbances can even become predominant over the corresponding varicose disturbances in the atomization process. In practice, atomization occurs invariably at high Weber numbers, while absolute instability of a circular liquid jet has been known to occur at relatively small Weber numbers, typically at a Weber number around 3, as shown by Li and Shen.[8] It has also been demonstrated[3,4] that the liquid-phase compressibility has a negligible effect on the jet instability process. Therefore, in this study, an investigation is carried out for both the temporal and spatial instability of a viscous incompressible liquid jet issuing into an inviscid compressible gas stream with three-dimensional disturbances. The significant effect of gas compressibility and liquid viscosity on the development of three-dimensional disturbances is highlighted.

Stability Analysis

Consider the instability process of a viscous liquid jet issuing from a round nozzle of radius a into an infinitely large, inviscid, moving, and compressible gas medium. The equations governing the motion of both the liquid and gas phases are the conservation of mass and momentum, which are in cylindrical coordinate

$$\frac{1}{r}\frac{\partial}{\partial r}(rU_{j,r}) + \frac{1}{r}\frac{\partial U_{j,\theta}}{\partial \theta} + \frac{\partial U_{j,z}}{\partial z} = 0 \tag{1}$$

$$\frac{\partial U_{j,z}}{\partial t} + (\boldsymbol{U}_j \cdot \nabla)U_{j,z} = -\frac{1}{\rho_j}\frac{\partial P_j}{\partial z} + \nu_j \nabla^2 U_{j,z} \tag{2}$$

$$\frac{\partial U_{j,r}}{\partial t} + (\boldsymbol{U}_j \cdot \nabla)U_{j,r} - \frac{U_{j,\theta}^2}{r} = -\frac{1}{\rho_j}\frac{\partial P_j}{\partial r} + \nu_j\left(\nabla^2 U_{j,r} - \frac{U_{j,r}}{r^2} - \frac{2}{r^2}\frac{\partial U_{j,\theta}}{\partial \theta}\right) \tag{3}$$

$$\frac{\partial U_{j,\theta}}{\partial t} + (\boldsymbol{U}_j \cdot \nabla)U_{j,\theta} + \frac{U_{j,r}U_{j,\theta}}{r} = -\frac{1}{\rho_j r}\frac{\partial P_j}{\partial \theta} + \nu_j\left(\nabla^2 U_{j,\theta} - \frac{U_{j,\theta}}{r^2} + \frac{2}{r^2}\frac{\partial U_{j,r}}{\partial \theta}\right) \tag{4}$$

where

$$(\boldsymbol{U}_j \cdot \nabla) = U_{j,r}\frac{\partial}{\partial r} + \frac{U_{j,\theta}}{r}\frac{\partial}{\partial \theta} + U_{j,z}\frac{\partial}{\partial z}$$

and the Laplacian operator is given by

$$\nabla^2 = \frac{\partial^2}{\partial r^2} + \frac{1}{r}\frac{\partial}{\partial r} + \frac{1}{r^2}\frac{\partial^2}{\partial \theta^2} + \frac{\partial^2}{\partial z^2}$$

The subscript $j = l$ represents quantities associated with the liquid phase, and $j = g$ represents the gas phase. The effect of gas viscosity is neglected, i.e., $\nu_g = 0$. The neglect of gas viscosity is based on the observation that the viscosity of the surrounding gas medium is only weakly stabilizing, and does not influence the relevant phenomenon appreciably, as Lin and Ibrahim[9] found in a related work. It has also been shown[10] that the shear waves at the liquid–gas interface caused by the growth of boundary layers play a secondary role in the jet breakup process (the effect is orders of magnitude smaller than those considered herein). The effect of gravity has been neglected because the Froude number involved is typically very large for practical liquid atomization applications.

To solve the governing equations for the gas phase, an equation of state is used, which relates the gas pressure and density by

$$\left(\frac{\partial P_g}{\partial \rho_g}\right)_s = c^2 \tag{5}$$

where the subscript s denotes an isentropic process.

Flowfield solutions to the governing equations [Eqs. (1–4)] must satisfy the kinematic and dynamic boundary conditions at the interface $r = \xi$, which are

$$U_{j,r} = \left(\frac{\partial}{\partial t} + \boldsymbol{U}_j \cdot \nabla\right)\xi \tag{6}$$

$$(\upsilon_l - \upsilon_g) \times \boldsymbol{n} = 0 \tag{7}$$

$$(\upsilon_l - \upsilon_g) \cdot \boldsymbol{n} + \sigma \nabla \cdot \boldsymbol{n} = 0 \tag{8}$$

where the subscript $j = l$ and g. The subscript r represents the radial component of the velocity vector in the cylindrical coordinate system (z, r, θ), whose origin is located at the nozzle exit, and whose axial coordinate z coincides with the jet centerline, and is positive in the flow direction.

The basic state that satisfies the governing equations and the boundary conditions is given by

$$\begin{gathered}\bar{\boldsymbol{U}}_l = (\bar{U}_z, \bar{U}_r, \bar{U}_\theta)_l = (U_l, 0, 0)\\ \bar{\boldsymbol{U}}_g = (\bar{U}_z, \bar{U}_r, \bar{U}_\theta)_g = (U_g, 0, 0)\\ \rho_g = \bar{\rho}_g,\ \bar{P}_l - \bar{P}_g = (\sigma/a)\ (\text{at} \quad \xi = a)\end{gathered} \tag{9}$$

where the overbar denotes the basic state quantities. It might be pointed out here that the base flowfield given earlier essentially represents a vortex-sheet approximation. This is reasonable, because in practical applications, the nozzle orifice length-to-diameter ratio is small, so that an almost uniform velocity distribution is obtained. As a result, this base flowfield has been used in almost all previous analysis of liquid jet instability.[3–8] To examine the stability of this basic state, it is perturbed with three-dimensional disturbances, such that the perturbed flowfields become

$$\begin{gathered}\boldsymbol{U}_j = \bar{\boldsymbol{U}}_j + \boldsymbol{u}_j, \qquad P_j = \bar{P}_j + p_j\\ \rho_g = \bar{\rho}_g + \rho_g', \qquad \xi = a + \eta\end{gathered} \tag{10}$$

where the lower-case symbols $\boldsymbol{u}$ and p are used to designate the perturbations of the flow velocity and pressure, respectively, ρ_g' represents the fluctuations in the gas density, and η is the displacement of the interface from the basic state cylindrical surface. It should be noted that $\rho_l = \bar{\rho}_l$ because the liquid phase has been assumed incompressible.

Substituting Eq. (10) into the governing Eqs. (1–4), canceling out the basic state solutions and neglecting the nonlinear terms, and utilizing Eq. (5) for the gas phase, we arrive at the following linearized equations for the perturbed flowfields:

$$\nabla \cdot \boldsymbol{u}_l = 0 \tag{11}$$

$$\rho_l\left(\frac{\partial}{\partial t} + U_l\frac{\partial}{\partial z}\right)\boldsymbol{u}_l = -\nabla p_l + \mu_l \nabla^2 \boldsymbol{u}_l \tag{12}$$

$$\frac{\partial p_g}{\partial t} + U_g\frac{\partial p_g}{\partial z} = -c^2\bar{\rho}_g \nabla \cdot \boldsymbol{u}_g \tag{13}$$

$$\bar{\rho}_g\left(\frac{\partial}{\partial t} + U_g\frac{\partial}{\partial z}\right)\boldsymbol{u}_g = -\nabla p_g \tag{14}$$

Clearly, the Coriolis and centrifugal force terms have vanished on the linearization. The corresponding linearized boundary conditions are, at $r = a$

$$u_{j,r} = \left(\frac{\partial}{\partial t} + U_j \frac{\partial}{\partial z}\right)\eta, \qquad (j = l, g) \tag{15}$$

$$\tau_{rz} = \mu_l \left(\frac{\partial u_{l,r}}{\partial z} + \frac{\partial u_{l,z}}{\partial r}\right) = 0 \tag{16}$$

$$\tau_{r\theta} = \mu_l \left[r\frac{\partial}{\partial r}\left(\frac{u_{l,r}}{r}\right) + \frac{1}{r}\frac{\partial u_{l,r}}{\partial \theta}\right] = 0 \tag{17}$$

$$p_l - 2\mu_l \frac{\partial u_{l,r}}{\partial r} - p_g + \frac{\sigma}{a^2}\left(1 + a^2\frac{\partial^2}{\partial z^2} + \frac{\partial^2}{\partial \theta^2}\right)\eta = 0 \tag{18}$$

To solve the governing equations [Eqs. (11–14)], we take the divergence of Eqs. (12) and (14), and utilizing Eqs. (11) and (13), we have

$$\nabla^2 p_l = 0 \tag{19}$$

$$\frac{\partial^2 p_g}{\partial t^2} + 2U_g \frac{\partial^2 p_g}{\partial z \partial t} + U_g^2 \frac{\partial^2 p_g}{\partial z^2} = c^2 \nabla^2 p_g \tag{20}$$

Note that Eq. (20) is just the convected wave equation.

The previous governing equations [Eqs. (19) and (20) together with Eqs. (11) and (13)] are solved in terms of the normal mode solution in the following form:

$$(\boldsymbol{u}_j, p_j, \eta) = [\tilde{\boldsymbol{u}}_j(r), \tilde{p}_j(r), \eta_0] \exp[\omega t + i(kz + n\theta)] \tag{21}$$

where η_0 is the initial amplitude of the interfacial disturbance, (k, n) are the wavenumber vector with n here being integer numbers, t is time, and $i = \sqrt{-1}$.

It may be pointed out that the interfacial waves on the jet surface with $n = 0$ correspond to two-dimensional symmetrical jet surface deformation with successive contraction and expansion in the radial direction, and are often referred to as varicose disturbances. Disturbances with $n = 1$ have jet surface deformations in which the cross section, while remaining circular, is displaced relatively to the jet axis, thus, the jet acquires a wavelike profile, which is usually called sinuous disturbances. For disturbances with $n = 2$, the jet develops elliptical cross sections. An ellipse with a horizontal major axis is transformed successively into an ellipse with a vertical major axis, and vice versa. For $n \geq 3$, sinusoidal surface deformations occur both in the axial and circumferential directions, and become increasingly complicated as unstable disturbances with larger values of n set in and start to grow on the jet surface. Figure 1 shows schematically various modes of disturbances.

The final bounded solutions to the governing differential equations [Eqs. (11–14)] are given next:

$$p_l = -\rho_l(\omega + ikU_l)A_1 I_n(kr) \exp[\omega t + i(kz + n\theta)]$$

$$u_{l,z} = [ikA_1 I_n(kr) + A_2 I_n(sr)] \exp[\omega t + i(kz + n\theta)]$$

$$u_{l,r} = [kA_1 I_n'(kr) - (ik/s)A_2 I_{n-1}(sr) + A_3(n/sr)I_n(sr)] \exp[\omega t + i(kz + n\theta)] \tag{22}$$

$$u_{l,\theta} = i[nA_1(1/r)I_n(kr) - (ik/s)A_2 I_{n-1}(sr) + A_3 I_n'(sr)] \exp[\omega t + i(kz + n\theta)]$$

$$p_g = -\bar{\rho}_g(\omega + ikU_g)BK_n(qr) \exp[\omega t + i(kz + n\theta)]$$

$$u_{g,r} = qBK_n'(qr) \exp[\omega t + i(kz + n\theta)]$$

where A and B are the integration constants; I_n and K_n are, respectively, the modified Bessel function of the first and second kinds,

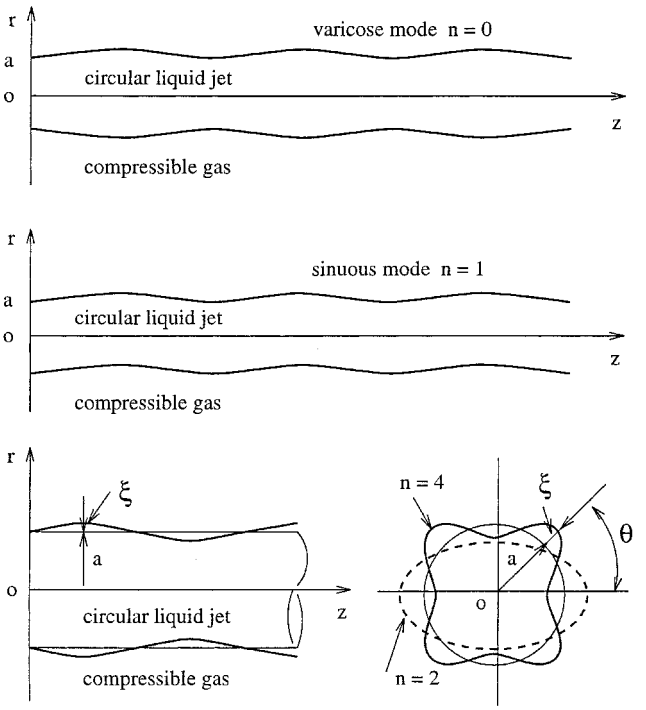

Fig. 1 Schematic of various modes of disturbances on liquid jet surface.

the prime represents the derivative with respect to the argument; and $s^2 = k^2 + (\omega + ikU_l)/\nu_l$, $q^2 = k^2 + (\omega + ikU_g)^2/c^2$. It should be noted that, in general, the only Bessel functions that can guarantee boundedness at infinity for complex arguments are Hankel functions. However, for the present problem, the modified Bessel functions are satisfactory for the gas-phase solutions because the wave number k is real for the temporal instability analysis, and the real part of the wave number is much larger than the imaginary part (at least one order of magnitude larger) for the spatial instability analysis, as shown later in the Results section. Therefore, other researchers have also used the modified Bessel functions for the gas-phase solutions.[3,4] Substitution of the previous solution into the boundary conditions [Eqs. (15–18)] results in the following dispersion relation, in dimensionless form:

$$\Omega_1^2\left(\frac{\Delta_1}{\Delta}\right) - \Omega_2^2\left[\frac{\rho}{q_a}\frac{K_n(q_a)}{K_n'(q_a)}\right] + 2Z\Omega_1\left\{m^2\frac{I_n''(m)}{I_n(m)}\frac{\Delta_1}{\Delta} - \frac{m^2}{s_a}\frac{I_{n-1}'(s_a)}{I_n'(s_a)}\left[1 + m\frac{I_n'(m)}{I_n(m)}\frac{\Delta_1}{\Delta}\right] - \frac{(s_a)I_n'(s_a) - I_n(s_a)}{I_n(s_a)} \times \left[m\frac{I_n'(m)}{I_n(m)}\frac{\Delta_1}{\Delta} - \left(\frac{m}{s_a}\right)^2\frac{I_{n-1}(s_a)}{I_n'(s_a)}\left(1 + m\frac{I_n'(m)}{I_n(m)}\frac{\Delta_1}{\Delta}\right) - 1\right]\right\} = 1 - m^2 - n^2 \tag{23}$$

where the dimensionless parameters are defined as follows: $\Omega = \omega(\rho_l a^3/\sigma)^{1/2}$, $\Omega_1 = \Omega + im\sqrt{(We)}$, $\Omega_2 = \Omega + imU\sqrt{(We)}$, $U = U_g/U_l$ is the velocity ratio of the gas to the liquid phase, $We = \rho_l U_l^2 a/\sigma$ is the liquid Weber number, $Z = \mu_l/(\rho_l a\sigma)^{1/2}$ is the Ohnesorge number, $\rho = \bar{\rho}_g/\bar{\rho}_l$ is the density ratio of the surrounding gas to the liquid, $m = ka$ is the axial wave number, and $M_a = U_l/c$ is the Mach number of the ambient gas with respect to a frame of reference moving with the jet at a velocity U_l. This choice for the Mach number is based on practical applications, such as in diesel fuel injection, where the liquid jet is typically injected at high velocities into a relatively slow-moving air medium, and the instability waves propagate from the wavy jet surface into the compressible gas stream.

Further, $q_a = \sqrt{\{m^2 + [\Omega/\sqrt{(We)} + imU]^2 M_a^2\}}$, $s_a = m^2 + \Omega_1/Z$, and

$$\Delta_1 = -n^2 + \frac{s_a}{I_n(s_a)}\left[2I_n'(s_a) - \left(s_a + \frac{n^2}{s_a}\right)I_n(s_a)\right] + \frac{(m)^2}{s_a I_n'(s_a)}\left\{n\left[I_{n-1}'(s_a) - \frac{I_{n-1}(s_a)}{s_a}\right] + \frac{I_{n-1}(s_a)}{I_n(s_a)} \times \left[2I_n'(s_a) - \left(s_a + \frac{n^2}{s_a}\right)I_n(s_a)\right]\right\} \quad (24)$$

$$\Delta = -2n^2 + (m)\frac{I_n'(m)}{I_n(m)} \times \left\{\frac{2s_a}{I_n(s_a)}\left[2I_n'(s_a) - \left(s_a + \frac{n^2}{s_a}\right)I_n(s_a)\right] - \Delta_1\right\} \quad (25)$$

For the varicose disturbances ($n = 0$), Eqs. (24) and (25) reduce to

$$\frac{\Delta_1}{\Delta} = \frac{I_0(m)}{(m)I_1(m)}\frac{s_a^2 + m^2}{s_a^2 - m^2} \quad (26)$$

Then Eq. (23) becomes, for the varicose disturbances ($n = 0$)

$$\Omega_1^2 + \Omega_2^2\left[\rho\frac{m}{q_a}\frac{K_0(q_a)}{K_1(q_a)}\frac{I_1(m)}{I_0(m)}\right] + 2Zm^2\Omega_1\left[1 + \frac{I_1'(m)}{I_0(m)}\right] + 4Z^2m^3\left[m\frac{I_1'(m)}{I_0(m)} - s_a\frac{I_1(m)}{I_0(m)}\frac{I_1'(s_a)}{I_1(s_a)}\right] = m\frac{I_1(m)}{I_0(m)}(1 - m^2) \quad (27)$$

It is clear that the gas-phase compressibility effect enters the dispersion relation through the gas-phase pressure fluctuations via the normal stress boundary condition. Hence, the rest of the terms in the dispersion relation remain the same as for the incompressible case, which has been given by Li.[7]

In the present analysis, disturbances are allowed to grow both temporally and spatially. The characteristics of disturbances are obtained by solving the dispersion relation with the specified flow parameters, such as We, M_a, Z, and ρ, and the effect of gas compressibility on the nature and growth of disturbances is investigated in terms of the Mach number, and the liquid viscous effect in terms of the Ohnesorge number Z. Numerical solutions are procured through Muller's method,[11] and the iteration is terminated when the relative error between the successive iterations for the eigenvalue (Ω in the temporal instability and m in the spatial instability calculations) satisfies a pre-set tolerance, which is usually 10^{-4} or less in the present study. Because the purpose and the interest of the present study are on the instability of liquid jets, only unstable solutions to the dispersion relation will be presented in the next section, although the same numerical technique is capable of determining stable solutions as well, which occur outside the unstable range of wave numbers given in this study.

Results and Discussion

Numerical results for both temporal and spatial instability have been obtained to fully understand the characteristics of instability development and liquid jet disintegration processes. Figure 2 shows the variation of the temporal wave growth rate Ω_r, with the wave number and Mach number for varicose disturbances at $We = 10^4$, $Z = 10^{-3}$, $\rho = 10^{-3}$, and $U_g = 0$. Here, the density ratio of $\rho = 10^{-3}$ represents the case of a water jet in air at room temperature, the Ohnesorge number of $Z = 10^{-3}$ implies a very mild viscous effect, and the velocity ratio of zero means that the jet is discharged into stationary ambient gas environment. These values of parameters are encountered in many common applications. It is seen that the growth rate as well as the dominant and cutoff wave

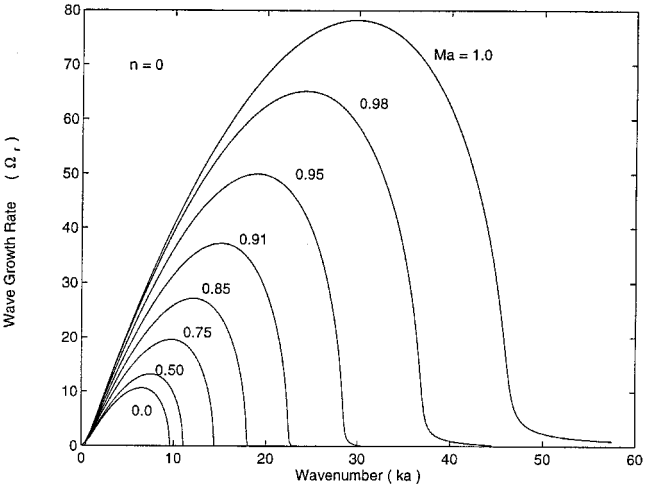

Fig. 2 Dimensionless temporal wave growth rate for varicose mode. $n = 0$, $We = 10^4$, $Z = 10^{-3}$, $\rho = 10^{-3}$, $U_g = 0$, and M_a, as shown.

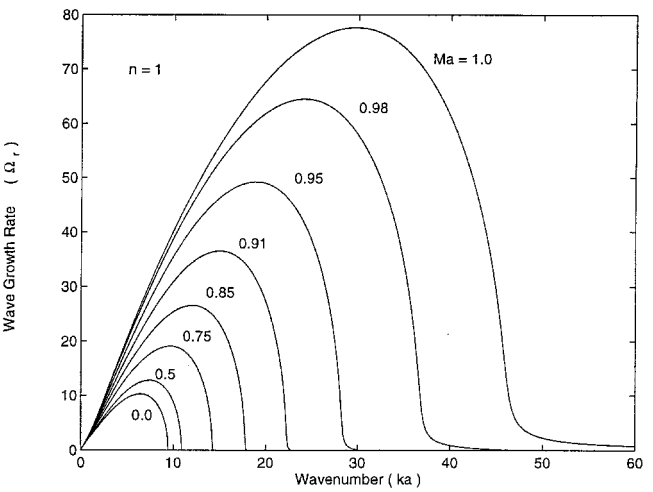

Fig. 3 Dimensionless temporal wave growth rate for sinuous mode. $n = 1$, $We = 10^4$, $Z = 10^{-3}$, $\rho = 10^{-3}$, $U_g = 0$, and M_a, as shown.

number change little for $M_a \leq 0.3$, and then increase rapidly with Mach number, particulary when the Mach number is close to 1. It is particularly noticeable that the cutoff wave number becomes extremely large near $M_a = 1$, and, in fact, it is infinitely large at unity Mach number. This result has been shown by Chawla,[12] in his study of a sonic gas jet submerged in a liquid, and is valid for all instabilities associated with a gas–liquid interface for liquids having finite viscosity. Therefore, a viscous liquid jet with unity M_a is unstable when subject to disturbances of all wavelengths, whether short or long, and it is because the pressure perturbation at the interface is always out of phase with the wave motion.

Figure 3 shows the temporal wave growth rate of the sinuous disturbance with the same values of flow parameters as those in Fig. 2. Clearly, the gas compressibility promotes the disturbance growth, and increases the dominant and cutoff wave number, just as for the varicose disturbances shown in Fig. 2. Similar results are given in Fig. 4 for the three-dimensional disturbance of $n = 2$. As shown by Li[7] for the incompressible case, two cutoff wave numbers exist for any three-dimensional disturbance with $n \geq 2$. The lower cutoff wave number is decreased slightly, whereas the upper cutoff wave number is increased significantly when the Mach number is increased. Both the lower and upper cutoff wave number owe their existence to the stabilizing effect of surface tension. As shown for Rayleigh instability,[13] i.e., a cylindrical, inviscid, low-speed liquid jet in a gas medium of negligible density, surface tension is unstable only for the axisymmetric varicose mode, i.e., $n = 0$, with axial

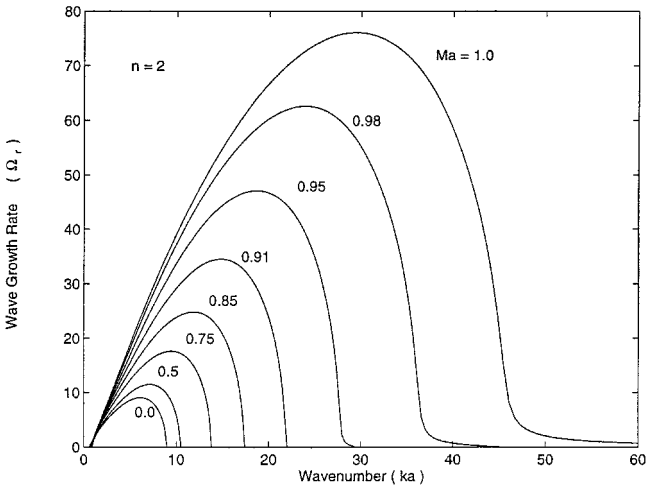

Fig. 4 Dimensionless temporal growth rate for mode $n = 2$. $We = 10^4$, $Z = 10^{-3}$, $\rho = 10^{-3}$, $U_g = 0$, and M_a, as shown.

wave numbers in the range of zero and the inverse of the jet radius, and it stabilizes all modes of disturbances with the azimuthal wave number $n \geq 1$. For the present case of liquid jets in a gas stream, the aerodynamic effect, further aided by the gas compressibility effect, destabilizes the jet for three-dimensional disturbances ($n \geq 1$), and increases the range of unstable wave numbers for each mode of disturbances. The results for $n > 2$ remain qualitatively the same as those for $n = 2$ under the same flow conditions, but as the value of n is increased, the lower cutoff wave number will become progressively larger, and the upper one gradually smaller, along with successively smaller growth rate. At sufficiently large values of n, the unstable range of the wave number disappears and the growth rate vanishes, so that a liquid jet will be stable for three-dimensional disturbances of sufficiently large values of the tangential wave number n under a given flow condition. A typical result can be found in Li[7] for $M_a = 0$.

Figure 5 illustrates the effect of the liquid viscosity (through the Ohnesorge number Z) for different Mach numbers. The results given in Fig. 5a correspond to $M_a = 0$, whereas those in Fig. 5b are for $M_a = 0.85$. The solid curves are for the two-dimensional disturbances of $n = 0$, and the dashed curves are for the three-dimensional disturbances of $n = 1$. It is seen that the gas compressibility enhances the instability of liquid jets, as discussed earlier. As the liquid viscous effect increases (or Z increases), the growth rate is reduced significantly for both two- and three-dimensional disturbances. However, the growth rate for $n = 0$ decreases faster than that for $n = 1$, such that at $Z = 1$ the growth rate for $n = 1$ becomes larger than the value for $n = 0$ for the incompressible case ($M_a = 0$), whereas the growth rate is comparable for the compressible case ($M_a = 0.85$). This indicates that the stabilizing effect of liquid viscosity has been reduced by the gas compressibility effects. Further calculations show that for larger values of Z, the growth rate for $n = 1$ will become predominant, suggesting that even with the presence of gas compressibility, the sinuous disturbances may still dominate the jet breakup process caused by the liquid viscous effect. It should be pointed out that over most of the unstable wave number range, the two-dimensional mode is still more unstable than the three-dimensional mode, and it is only at very long wavelengths that the three-dimensional modes become more unstable for highly viscous liquids.

The typical effect of gas-to-liquid density ratio on the temporal growth rate is illustrated in Fig. 6 for $We = 5000$, $Z = 10^{-3}$, $M_a = 0.85$, $U_g = 0$, and $n = 0$. It is clear that the gas density increases the disturbance growth rate, and dominant and cutoff wave numbers, indicating the destabilizing effect of gas density. Figure 7 shows the effect of the gas velocity, normalized by the liquid jet velocity, on the temporal instability for $n = 0$, $We = 36.598$, $Z = 1.096 \times 10^{-3}$, $\rho = 1.74 \times 10^{-4}$, and $M_a = 1.023$. It is interesting to note that when the liquid jet is injected into a stationary gas medium ($U_g = 0$), the wave growth rate shows only one peak, which represents the surface tension effect dominating the instability

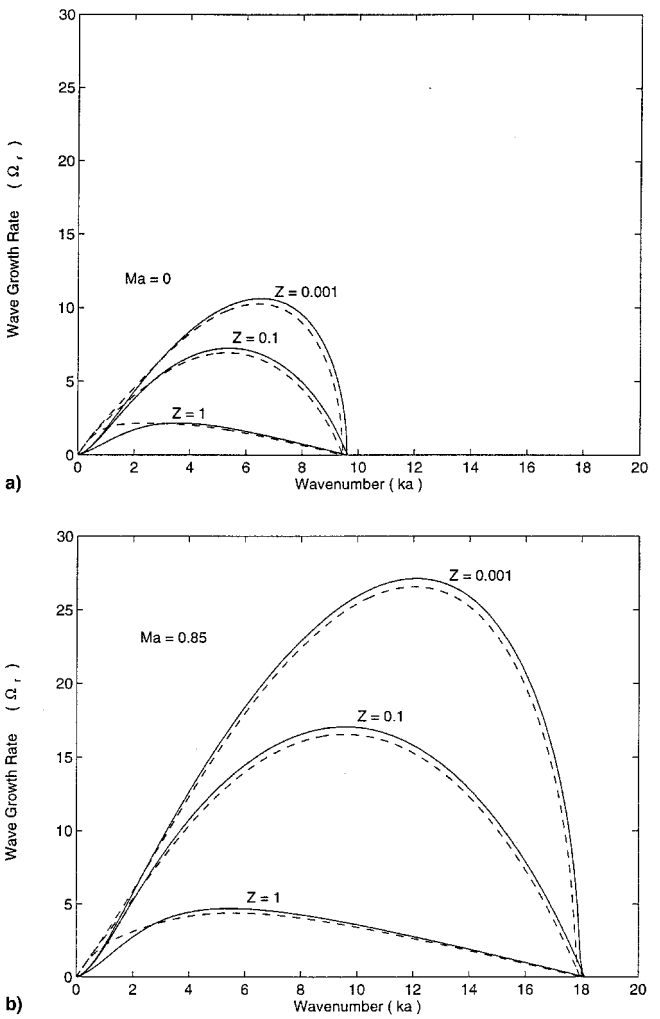

Fig. 5 Liquid viscous effects on the dimensionless temporal wave growth rate. $We = 10^4$, $\rho = 10^{-3}$, and $U_g = 0$. Solid curves: $n = 0$; dashed curves: $n = 1$. M_a = a) 0 and b) 0.85.

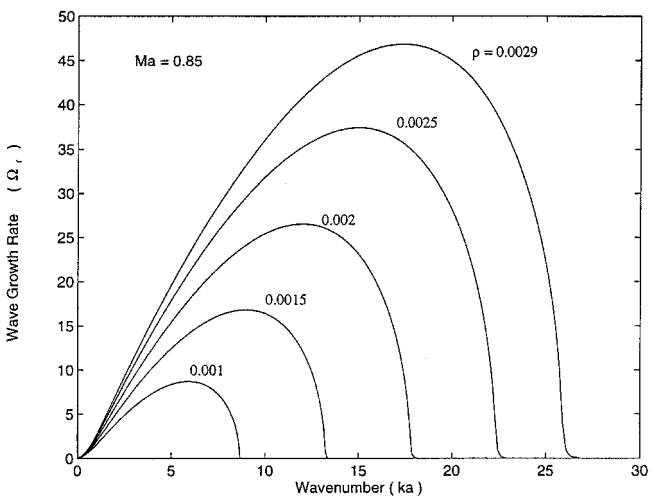

Fig. 6 Effects of gas-to-liquid density ratio on the dimensionless temporal wave growth rate for $n = 0$, $We = 5000$, $Z = 10^{-3}$, $M_a = 0.85$, $U_g = 0$, and ρ, as shown.

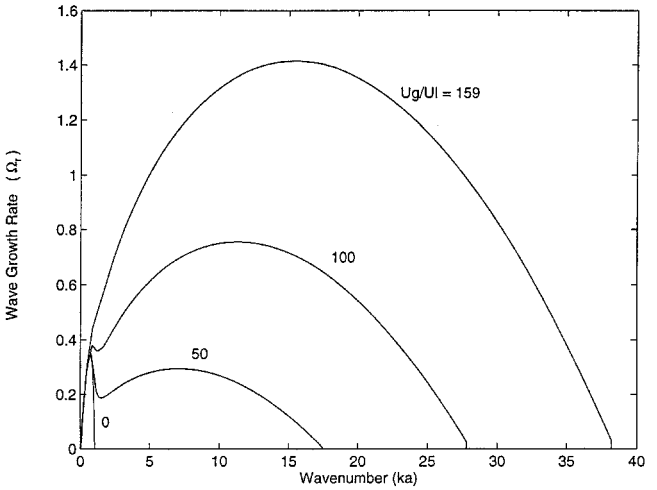

Fig. 7 Effects of gas-to-liquid velocity ratio on the temporal wave growth rate. $n = 0$, $We = 36.598$, $Z = 1.096 \times 10^{-3}$, $\rho = 1.74 \times 10^{-4}$, $M_a = 1.023$, and U_g, as shown.

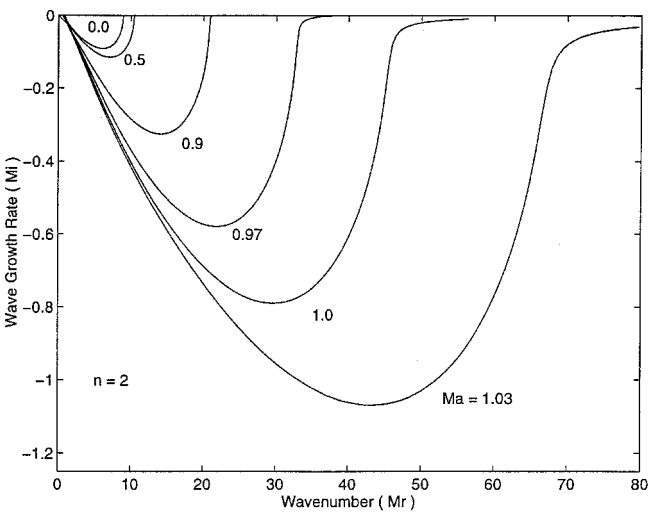

Fig. 8 Dimensionless spatial wave growth rate for $n = 2$, $We = 10^4$, $Z = 10^{-3}$, $\rho = 10^{-3}$, $U_g = 0$, and M_a, as shown.

process. When $U_g = U_l$, the jet instability is essentially reduced to the well-known Rayleigh instability, for which surface tension is the only source of instability. However, when the gas velocity is increased, a second peak of the wave growth rate appears, along with a considerable increase in the cutoff wave number. This second peak is a result of the enhanced aerodynamic interactions between the liquid and gas phase, and it increases with the gas velocity. Therefore, for sufficiently large gas velocities, the second peak becomes larger than the first peak with a sudden increase in the dominant wave number. Because the diameter of the droplets formed from the jet breakup is directly related to the dominant wavelength, a suitable coflowing gas stream can significantly enhance the quality of atomization.

For spatial instability, the wave frequency Ω in the dispersion relation, Eqs. (23) and (27), is taken as pure imaginary, i.e., $\Omega = -i\Omega_i$ with Ω_i representing the wave frequency, and the axial wave number m becomes complex, $m = m_r + im_i$, where m_r represents the wave number, and $-m_i$ the spatial wave growth rate. Figure 8 gives the typical spatial growth rate m_i against the wave number m_r with different Mach numbers. As for the temporal case, the results also indicate significant effects of the gas compressibility. In fact, it can be shown that the results of temporal instability and those of spatial instability are related by Gaster's relation,[14] which states that the spatial growth rate is related to the temporal growth rate by the group velocity. For the present liquid jet instability, the group velocity, as shown in Fig. 9, is almost exactly the same as the liquid

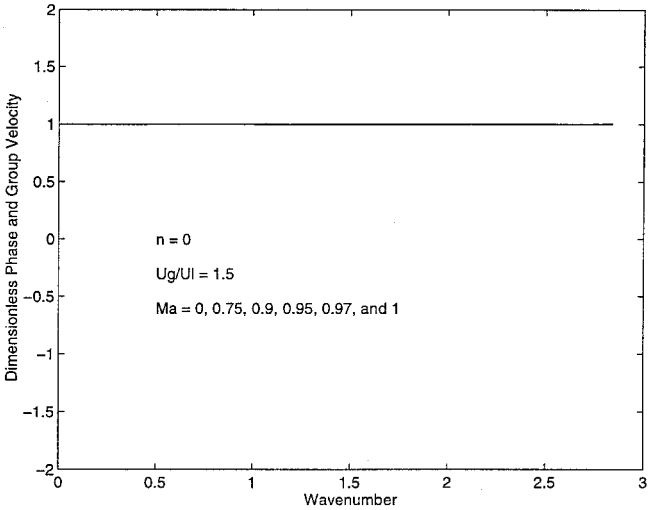

Fig. 9 Phase and group velocity of waves, normalized by the liquid jet velocity, for various Mach numbers. $We = 10^4$, $Z = 10^{-3}$, $\rho = 10^{-3}$, $U_g/U_l = 1.5$, and $n = 0$. The unstable wave number range can be inferred from Fig. 10b for different Mach numbers.

jet velocity. Hence, results similar to the temporal instability presented earlier are obtained for the effects of gas compressibility, liquid viscosity, and density ratio on the spatial instability. Figure 9 also indicates that both group velocity and phase velocity are the same, and equal to the liquid jet velocity, and they are almost independent of other flow parameters. Therefore, the surface waves are subsonic as long as the Mach number is less than 1. This result is representative of all the cases investigated in the present study.

It might be pointed out that the Gaster relation[14] was derived for nearly parallel flows (such as boundary-layer flows), where growth rates are typically small; it is also valid for the present case of liquid jet instability, although the growth rates may be very large. A typical result is shown in Fig. 10 for the flow conditions of $We = 10^4$, $Z = 10^{-3}$, $\rho = 10^{-3}$, and $n = 0$. Figure 10a is for the gas stream velocity of $U_g = 0$, under which the growth rates are large (on the order of one), and Fig. 10b for $U_g/U_l = 1.5$, where the growth rates are relatively small because of reduced aerodynamic effects resulting from a smaller velocity difference between the liquid and gas stream. The solid curves represent the spatial growth rate, and the dashed curves are the temporal growth rate at the same condition transformed according to Gaster relation. It is seen from Fig. 10a that both the solid and dashed curves coincide with each other for Mach numbers as high as 0.9, and the difference for higher Mach numbers is still small, barely noticeable around the maximum growth rates. The agreement between the temporal and spatial results is even better for smaller growth rates, as shown in Fig. 10b, where the only noticeable, yet still small, difference lies around the cutoff wave numbers. Gaster relation has also been shown, by asymptotic analysis, to be valid for Rayleigh instability at relatively large Weber numbers.[15]

The dominant wave number, which corresponds to the maximum growth rate for a given set of flow conditions, is of practical importance in atomization process, because it relates to the diameter of the subsequently formed droplets after the liquid jet disintegrates. Because the spatial instability results can be determined from the corresponding temporal ones through Gaster's relation, only the dominant wave number of the temporal instability is presented here for varicose disturbances. Figure 11 shows the dominant wave number as a function of Weber and Mach numbers. It is seen that the dominant wave number increases rapidly with both We and M_a, particularly at large values of We and M_a. Also notice that the increase for $M_a \leq 0.3$ is fairly small, as may be expected. On the other hand, increasing viscous effects reduces the dominant wave number, as shown in Fig. 12. Obviously, the viscous effect is more complex than the effect of surface tension and gas compressibility when Fig. 12 is compared with Fig. 11. The results shown in Figs. 11 and

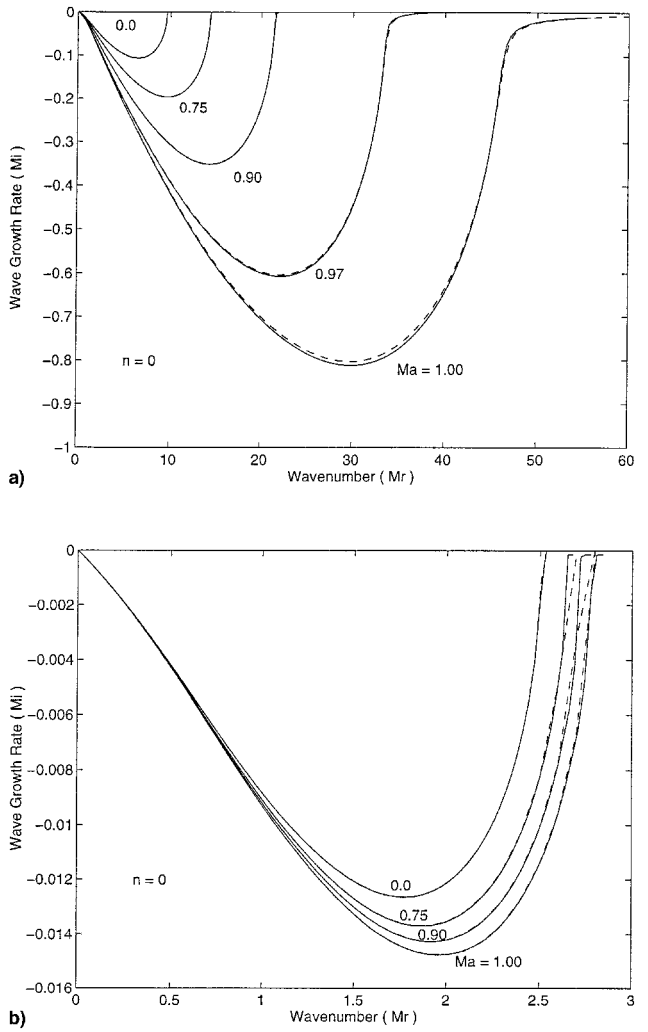

Fig. 10 Comparison between the spatial and temporal growth rates. $We = 10^4$, $Z = 10^{-3}$, $\rho = 10^{-3}$, and $n = 0$. Solid curves: spatial growth rate; dashed curves: temporal growth rate transformed according to Gaster relation.[14] U_g = a) 0 and b) $U_g/U_l = 1.5$.

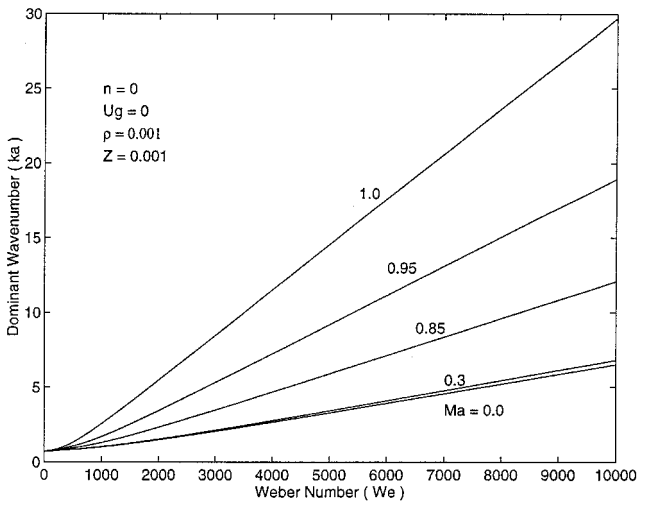

Fig. 11 Dominant wave number of temporal instability as a function of Weber number and Mach number. $n = 0$, $Z = 10^{-3}$, $\rho = 10^{-3}$, and $U_g = 0$.

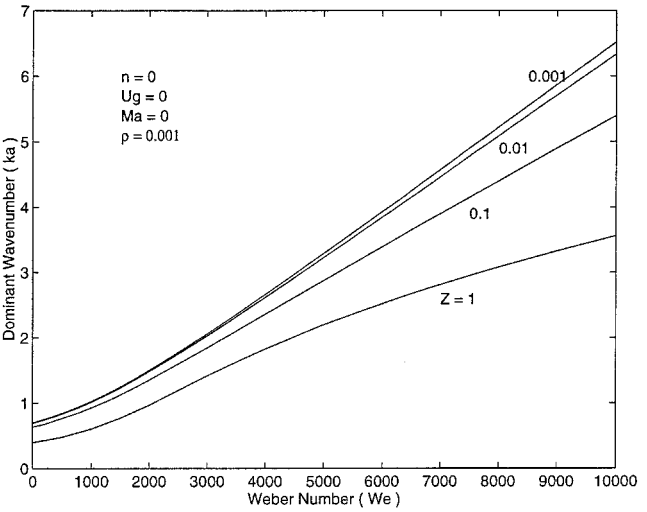

Fig. 12 Dominant wave number of temporal instability as a function of Weber number and Ohnesorge number. $n = 0$, $\rho = 10^{-3}$, $U_g = 0$, and $M_a = 0$.

12 indicate that increasing Weber number and gas compressibility and reducing liquid viscous effect can all contribute to the reduction of droplet size in sprays.

Finally, it might be pointed out that the present analysis is not restricted to the case of $M_a \leq 1$. In fact, other workers, e.g., Refs. 3–5, have applied a similar analysis to the case of $M_a > 1$. However, such application for $M_a > 1$ should be cautioned as experimental evidences[2] suggest the appearance of shock waves in the ambient gas phase, thus invalidating the base flowfield assumed in the analysis. Hence, we have restricted the presentation of the results for the Mach numbers up to slightly larger than one.

Conclusions

This study investigates the temporal and spatial instability of a viscous liquid jet discharged into an inviscid compressible gas medium with three-dimensional disturbances. It is shown that for $M_a > 0.3$ the gas compressibility enhances the growth rate for both two- and three-dimensional disturbances considerably, widens the range of unstable wave numbers, and promotes significantly the jet disintegration process, especially when close to the sonic region. For viscous liquids, sinuous disturbances may become the most unstable mode of disturbances under certain flow conditions. The density ratio of gas-to-liquid increases the disturbance growth rate, and dominant and cutoff wave numbers. The gas velocity can significantly enhance the liquid jet breakup process and improve the quality of atomization.

Acknowledgments

This work is supported by the Natural Sciences and Engineering Research Council of Canada. The financial support of the China Association for International Exchange of Personnel, via scholarship to T. Chen, is gratefully acknowledged.

References

[1]Lefebvre, A. H., *Atomization and Sprays*, Hemisphere, New York, 1989.

[2]Shi, H. H., Takayama, K., and Onodera, O., "Experimental Study of Pulsed High-Speed Liquid Jet," *JSME International Journal, Series B*, Vol. 36, No. 4, 1993, pp. 620–627.

[3]Zhou, Z. W., and Lin, S. P., "Effects of Compressibility on the Atomization of Liquid Jets," *Journal of Propulsion and Power*, Vol. 8, No. 4, 1992, pp. 736–740.

[4]Zhou, Z. W., and Lin, S. P., "Absolute and Convective Instability of a Compressible Jet," *Physics of Fluids A*, Vol. 4, No. 2, 1992, pp. 277–282.

[5]Li, H. S., and Kelly, R. E., "The Instability of a Liquid Jet in a Compressible Airstream," *Physics of Fluids A*, Vol. 4, No. 10, 1992, pp. 2162–2168.

[6]Lian, Z. W., and Reitz, R. D., "The Effect of Vaporization and Gas Compressibility on Liquid Jet Atomization," *Atomization and Sprays*, Vol. 3, No. 2, 1993, pp. 249–264.

[7]Li, X., "Mechanism of Atomization of a Liquid Jet," *Atomization and*

Sprays, Vol. 5, No. 1, 1995, pp. 89–105.

[8]Li, X., and Shen, J., "Absolute and Convective Instability of Cylindrical Liquid Jets in Co-Flowing Gas Streams," *Atomization and Sprays*, Vol. 8, No. 1, 1998, pp. 45–62.

[9]Lin, S. P., and Ibrahim, E. A., "Stability of a Viscous Liquid Jet Surrounded by a Viscous Gas in a Vertical Pipe," *Journal of Fluid Mechanics*, Vol. 218, Sept. 1990, pp. 641–658.

[10]Lin, S. P., and Lian, Z. W., "Mechanisms of the Breakup of Liquid Jets," *AIAA Journal*, Vol. 28, No. 1, 1990, pp. 120–126.

[11]Muller, D. E., "A Method for Solving Algebraic Equations Using an Automatic Computer," *Mathematical Tables and Other Aid to Computation*, Vol. 10, No. 5, 1956, pp. 208–215.

[12]Chawla, T. C., "The Kelvin–Helmholtz Instability of the Gas–Liquid Interface of a Sonic Gas Jet Submerged in a Liquid," *Journal of Fluid Mechanics*, Vol. 67, Pt. 3, 1975, pp. 513–537.

[13]Rayleigh, L., "On the Instability of Jets," *Proceedings of the London Mathematical Society*, Vol. 10, 1879, pp. 4–13.

[14]Gaster, M., "A Note on the Relation Between Temporally-Increasing and Spatially-Increasing Disturbances in Hydrodynamic Stability," *Journal of Fluid Mechanics*, Vol. 14, Pt. 2, 1962, pp. 222–224.

[15]Keller, J. B., Rubinow, S. I., and Tu, Y. O., "Spatial Instability of a Jet," *Physics of Fluids*, Vol. 16, Dec. 1973, pp. 2052–2055.